

1310nm silicon evanescent laser

Hsu-Hao Chang¹, Alexander W. Fang¹, Matthew N. Sysak¹, Hyundai Park¹, Richard Jones², Oded Cohen³, Omri Raday³, Mario J. Paniccia², and John E. Bowers¹

¹University of California, Santa Barbara, Department of Electrical and Computer Engineering, Santa Barbara, CA 93106, USA

²Intel Corporation, 2200 Mission College Blvd, SC12-326, Santa Clara, California 95054, USA

³Intel Corporation, S.B.I. Park Har Hotzvim, Jerusalem, 91031, Israel

Email: hsuhaochang@umail.ucsb.edu

Abstract: We report the first 1310 nm hybrid laser on a silicon substrate. This laser operates continuous wave (C.W.) up to 105 °C. The room temperature threshold current of this laser is 30 mA, and the maximum single sided fiber-coupled output power is 5.5 mW.

©2007 Optical Society of America

OCIS codes: (140.5960) Semiconductor lasers; (250.5300) Photonic integrated circuits.

References and links

1. H. Rong, R. Jones, A. Liu, O. Cohen, D. Hak, A. W. Fang, and M. Paniccia, "A continuous-wave Raman silicon laser," *Nature* **433**, 725-728 (2005).
2. O. Boyraz and B. Jalali, "Demonstration of a silicon Raman laser," *Opt. Express* **12**, 5269-5273 (2004).
3. A. W. Fang, H. Park, O. Cohen, R. Jones, M. J. Paniccia, and J. E. Bowers, "Electrically pumped hybrid AlGaInAs-silicon evanescent laser," *Opt. Express*, **14**, 9203-9210 (2006).
4. G. Roelkens, D. Van Thourhout, R. Baets, R. Nötzel, and M. Smit, "Laser emission and photodetection in an InP/InGaAsP layer integrated on and coupled to a Silicon-on-Insulator waveguide circuit," *Opt. Express* **14**, 8154-8159 (2006).
5. P. Rojo Romeo, J. Van Campenhout, P. Regreny, A. Kazmierczak, C. Seassal, X. Letartre, G. Hollinger, D. Van Thourhout, R. Baets, J. M. Fedeli, and L. Di Cioccio, "Heterogeneous integration of electrically driven microdisk based laser sources for optical interconnects and photonic ICs," *Opt. Express* **14**, 3864-3871 (2006).
6. R. Sawada, H. Nakada, and F. Ohira, "Highly accurate and quick bonding for planar lightwave circuit and laser-diode chip," in *Proceedings of IEEE IEMT/IMC* (IEEE, 1998), 133-137.
7. R. Boudreau, P. Zhou, and T. Bowen, "Wafer scale photonic-die attachment," *IEEE transactions on components, packaging and manufacturing technology, Part B* **21**, 136-139 (1998)
8. A. W. Fang, R. Jones, H. Park, O. Cohen, O. Raday, M. J. Paniccia, and J. E. Bowers, "Integrated AlGaInAs-silicon evanescent race track laser and photodetector," *Opt. Express* **15**, 2315-2322 (2007).
9. D. Pasquariello, and K. Hjort, "Plasma-assisted InP-to-Si low temperature wafer bonding," *IEEE J. Sel. Top. Quantum Electron.* **8**, 118-131 (2002).
10. Y.-A. Chang, T.-S. Ko, J.-R. Chen, F.-I. Lai, C.-L. Yu, I.-T. Wu, H.-C. Kuo, Y.-K. Kuo, L.-W. Lai, L.-H. Lai, T.-C. Lu, and S.-C. Wang, "The carrier blocking effect on 850 nm InAlGaAs/AlGaAs vertical-cavity surface-emitting lasers," *Semicond. Sci. Technol.* **21**, 1488-1494 (2006).
11. Fimmwave, Photon Design, <http://www.photond.com>
12. H. Park, A. W. Fang, O. Cohen, R. Jones, M. J. Paniccia, and J. E. Bowers, "A Hybrid AlGaInAs-Silicon Evanescent Amplifier," *IEEE Photon. Technol. Lett.* **19**, 230-232., (2007).

1. Introduction

Many advancements have been made in silicon photonics in recent years [1-5]. However, due to its indirect bandgap, an efficient laser source on silicon is a challenge for silicon photonics. Many efforts have been made to achieve lasers that are compatible with silicon, such as stimulated Raman scattering (SRS) [1,2] and heterogeneous integration of III-V materials [6,7]. But these methods either need external optical pumping source or need a precise alignment during the process. Bonding III-V layers directly to the passive optical circuits before III-V patterning has been used to overcome the alignment requirement of die attachment approaches [4,5]. Recently, silicon evanescent lasers (SELs) have been demonstrated in the 1.55 μm regime [3,8] and provide a solution for a highly scalable and electrically pumped laser on silicon. These lasers utilize a III-V quantum well active layer

bonded to a silicon waveguide to achieve optical gain. The optical mode of this hybrid waveguide lies in both the III-V region and the silicon waveguide. The optical mode is defined by the silicon waveguide and no alignment is needed during the bonding process. This allows for a large number of SELs to be fabricated to the silicon wafer through a single bonding step. All the previous SEL lasers were designed to operate at 1.5 μm wavelength. However, 1.3 μm lasers are also important for many communication networks because of their thermal performance and dispersion characteristics of optical fibers. Data transmission using 1.3 μm wavelength suffers less from signal dispersion because optical fibers have lower dispersion in the 1.3 μm wavelength regime than the 1.5 μm wavelength regime. We report an SEL operating at the wavelength of 1310 nm with a threshold current of 30 mA, maximum C.W. operating temperature of 105 $^{\circ}\text{C}$, and maximum single sided fiber-coupled output power of 5.5 mW.

2. Device structure

The device structure of a SEL is as shown in Fig. 1. The silicon wafer is fabricated with a set of rib waveguides on it. These rib waveguides have waveguide width (w) = 2.5 μm , height (h) = 0.69 μm , and rib etch depth (d) = 0.52 μm , as shown in Fig. 1. The device length is 860 μm . A detailed process description can be found in [3,8].

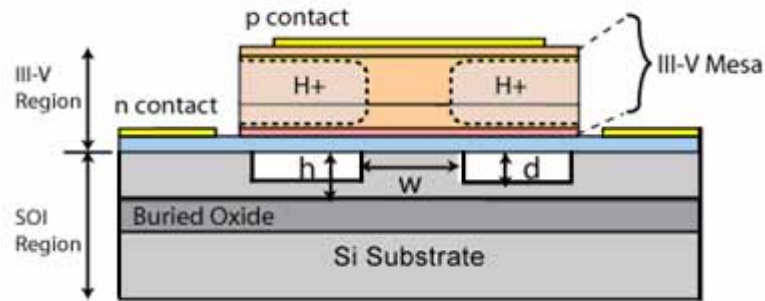


Fig. 1. Silicon evanescent laser structure. $w = 2.5 \mu\text{m}$, $h = 0.69 \mu\text{m}$, and $d = 0.52 \mu\text{m}$.

The III-V epitaxial structure is summarized in Table 1. The AlGaInAs quantum wells have a photo-luminescence peak at 1303 nm. The quantum wells are located between a n-layer and an electron blocking layer. The carrier blocking layer is designed to provide a high conduction band offset between the barrier and the SCH layer to prevent electrons from leaking out of the quantum well region, while having a low valence band offset to allow holes flow into the quantum well region [10].

Table 1. III-V epitaxial growth layer structure

III-V Epitaxial growth layer structure			
Name	Composition	Doping Concentration	Thickness
P contact layer	P-type $\text{In}_{0.53}\text{Ga}_{0.47}\text{As}$	$1 \times 10^{19} \text{ cm}^{-3}$	0.1 μm
Cladding	P-type InP	$1 \times 10^{18} \text{ cm}^{-3}$	0.5 μm
SCH	P-type $\text{Al}_{0.4055}\text{Ga}_{0.064}\text{In}_{0.5305}\text{As}$, 0.9 μm	$1 \times 10^{17} \text{ cm}^{-3}$	0.25 μm
Electron Blocking Layer	$\text{Al}_{0.4764}\text{Ga}_{0.0189}\text{In}_{0.5047}\text{As}$	undoped	10 nm
Quantum Wells	$\text{Al}_{0.178}\text{Ga}_{0.1234}\text{In}_{0.6986}\text{As}$, 1.5 μm (8x)	undoped	7 nm
	$\text{Al}_{0.055}\text{Ga}_{0.292}\text{In}_{0.653}\text{As}$, 1 μm (9x)	undoped	9 nm
N layer	N-type InP	$1 \times 10^{18} \text{ cm}^{-3}$	110 nm
Super Lattice	N-type $\text{In}_{0.85}\text{Ga}_{0.15}\text{As}_{0.327}\text{P}_{0.673}$ (2x)	$1 \times 10^{18} \text{ cm}^{-3}$	7.5 nm
	N-type InP (2x)	$1 \times 10^{18} \text{ cm}^{-3}$	7.5 nm

3. Experiment and results

The device is mounted on a thermal-electrical cooler and driven with a C.W. or pulsed current source. The laser output power is measured from one facet of the device with a single mode lensed fiber while monitoring the lasing mode on the other facet by using an infrared camera. The coupled light to the lensed fiber is sent to an optical spectrum analyzer or a photodetector to measure the output spectrum or the output power. The coupling loss of the single mode lensed fiber was estimated to be $\sim 4.6 \pm 0.8$ dB by using an integrating sphere

Figure 2(a) shows the measured SEL optical mode, and Fig. 2(b) and Fig. 2(c) show the simulated mode profiles for the fundamental mode and the second transverse optical mode of this structure for devices with 2.5 μm waveguide width. These modes are calculated by the film mode matching (FMM) method [11]. The quantum well confinement factors for the fundamental mode and second transverse mode are 2.2 % and 10.5 % while the silicon confinement factors for the fundamental mode and second transverse mode are 81 % and 34 %. Since the second transverse mode has a higher confinement factor in the III-V active region, it lases over the fundamental mode and was consistently observed (Fig. 2(a)).

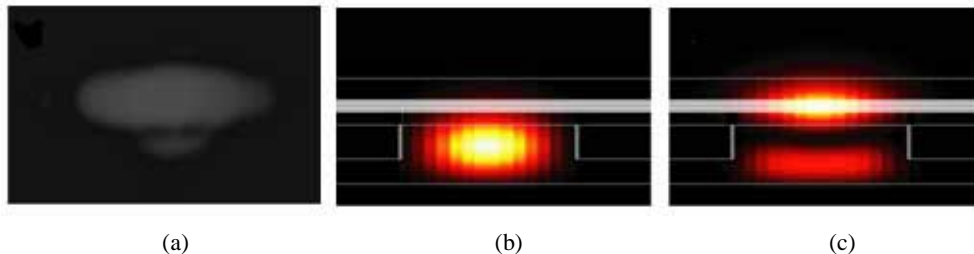


Fig. 2. The measured SEL optical mode and simulated results: (a) measured optical mode; (b) simulated fundamental mode; (c) second order transverse mode

Figure 3(a) shows the quantum well confinement factor as a function of silicon waveguide height (h in Fig. 1). In the tall silicon height regime (right hand part in Fig. 3(a)), a higher quantum well confinement factor for the second transverse mode exists. In the short silicon height regime (left hand part in Fig. 3(a)), the fundamental mode has a higher quantum well confinement factor. Fig. 3(b) shows the fundamental mode and second transverse mode for the tall silicon height regime (top figures), the crossover point (middle figures), and the short silicon height regime (bottom figures). As the silicon height decreases, the mode increasingly lies more in the III-V region. This drives the confinement factor of the fundamental mode up at the expense of coupling efficiency to non-hybrid silicon rib waveguide regions. The second transverse mode also undergoes an increase in III-V confinement factor but splits into two lateral lobes at lower silicon heights. This splitting reduces the modal overlap with the 4

micron wide excited quantum well region at the center, leading to lower confinement factors so that when the silicon height is less than $0.4 \mu\text{m}$, the fundamental mode will lase first.

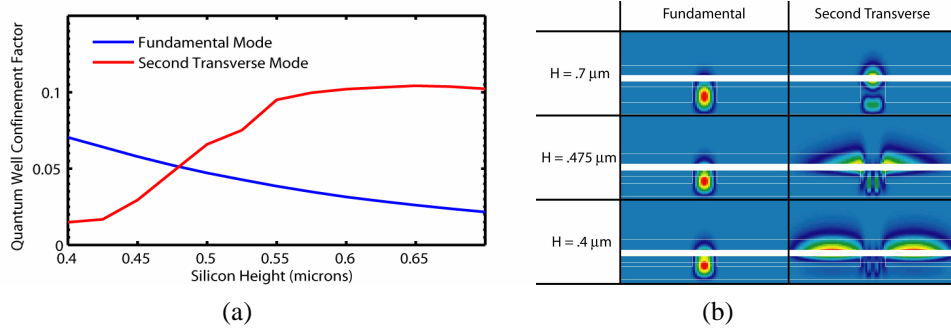


Fig. 3. The confinement factor in III-V region simulation for different silicon waveguide height: (a) confinement factor calculations for the fundamental mode and second transverse mode as a function of waveguide height (b) fundamental and second transverse modes for waveguide heights of 0.7, 0.475, and $0.4 \mu\text{m}$. The image aspect ratio (Height:Width) is 4:1.

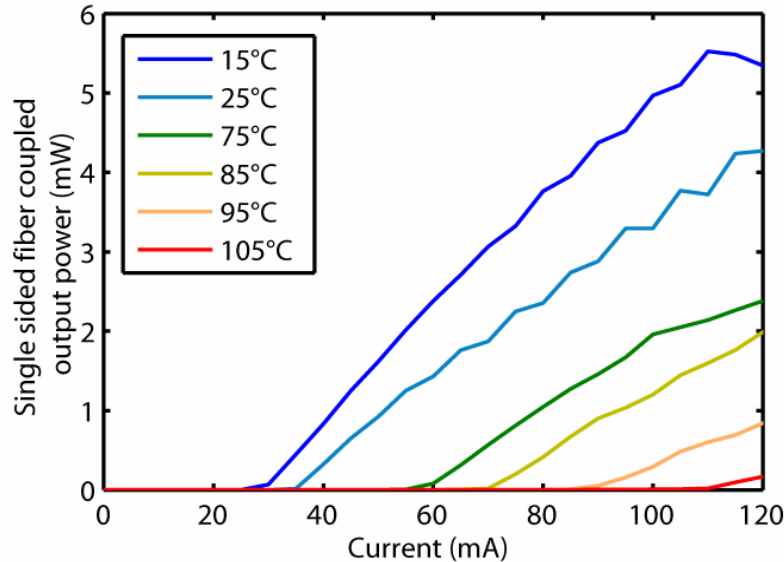


Fig. 4. The single sided fiber coupled laser power output as a function of drive current at different temperatures.

Figure 4 shows the measured single sided fiber coupled C.W. laser output power as a function of the injected current for various temperatures ranging from 15°C to 105°C . The turn on voltage at 15°C is 1.2V and the series resistance is 11.5 ohm . As shown in Fig. 4, the threshold current of the device at 15°C is 30 mA , which is 35 mA lower than previous SELs [3]. This is because the device lases at second transverse mode and it has higher confinement factor in the III-V active region. The highest operating temperature is 105°C . This is 50°C higher than the previous record [8]. This is because our lasing mode has larger quantum well confinement factor and the quantum wells are designed to have a larger conduction band offset than the design used in [8]. Moreover, it is generally known that $1.3 \mu\text{m}$ lasers have better thermal performance because of the reduced intravalence band absorption and Auger

scattering. The maximum output power measured by a single mode lensed fiber is 5.5 mW and the corresponding differential quantum efficiency is 8 %. Taking into account the fiber coupling loss and the lights from both sides of the facet, we estimate the total output power and differential quantum efficiency to be 31.6 mW and 46 %, respectively.

The characteristic temperature of the threshold (T_0) was 60 K and differential efficiency (T_1) was 112 K, as measured by a pulse current source with a repetition rate of 1 kHz and pulse width of 500 nsec,. Fig. 5(a) shows $1/\eta_d$ (η_d : differential quantum efficiency) at different device lengths. By linearly fitting this data, the injection efficiency and modal loss are estimated to be 52 % and 6.4 cm^{-1} respectively. The modal gain at different current densities for $2.5 \text{ }\mu\text{m}$ waveguide width was also measured from current thresholds of different device lengths. The modal gain was estimated to be $\sim 24 \text{ cm}^{-1}$ at the current density of 2000 A/cm^2 .

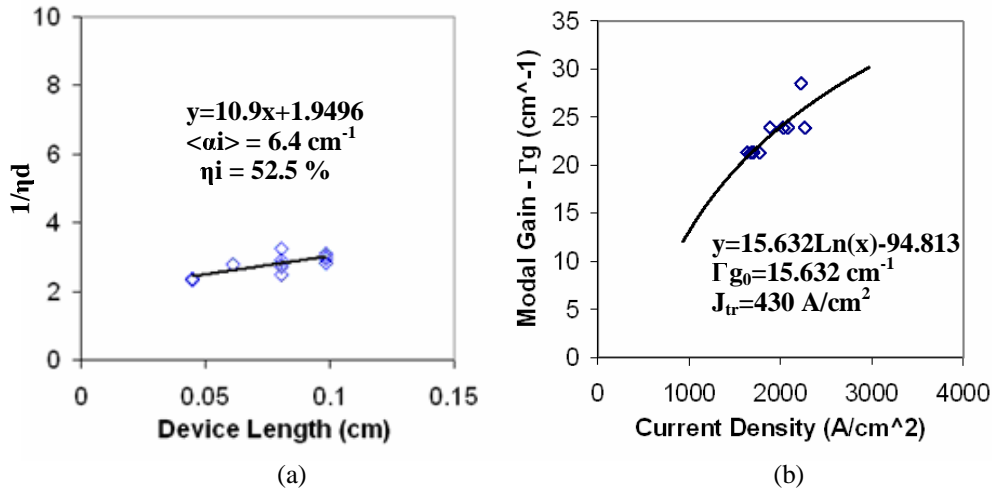


Fig. 5. Pulse measurement results for $2.5 \text{ }\mu\text{m}$ waveguide width SELs: (a) the relation between $1/\eta_d$ (differential quantum efficiency) and device length; (b) modal gain at different current densities.

Figure 6 shows the measured lasing spectrum of the SEL under 100 mA drive current at $15 \text{ }^\circ\text{C}$. The center wavelength is 1326 nm . The inset of Fig. 6 shows a close up of the lasing spectrum, showing the Fabry-Perot modes. The mode spacing is measured to be 0.27 nm , which corresponds to a group index of 3.83.

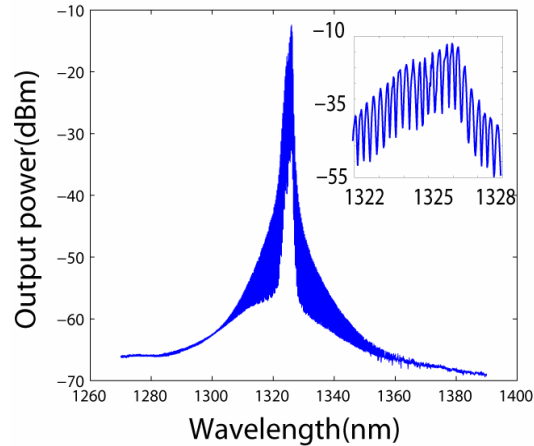


Fig. 6. The spectrum of silicon evanescent laser under 100 mA driving current at 15 °C.

4. Conclusions

Here we demonstrate the first electrically pumped 1310 nm hybrid laser on silicon. This laser lases at second transverse mode with a III-V quantum well confinement factor of 10.5 %. A low threshold current of 30 mA was demonstrated, and the maximum single sided fiber coupled output power was 5.5 mW. The single sided fiber coupled differential quantum efficiency is 8 % and the maximum lasing temperature is 105 °C. Taking into account the fiber coupling loss and the lights from both sides of the facet, the total output power and differential quantum efficiency are estimated to be 31.6 mW and 46 %, respectively. We can integrate a large number of these lasers on a single chip using only one bonding process. This technology is applicable to semiconductor optical amplifiers [12] at 1.3 μm , which is important because it is outside the wavelength range of erbium doped fiber amplifiers.

Acknowledgment

The authors thank Jag Shah, Michael Haney, Hui-Wen Chen, Gehong Zeng, and Ying-Hao Kuo for useful discussions. The UCSB research was supported by DARPA contracts W911NF-05-1-0175 and W911NF-04-9-0001, and by Intel.